Author Manuscript

Author Manuscript

Author Manuscript

Author Manuscript

HHS Public Access

Author manuscript

J Biomed Mater Res A. Author manuscript; available in PMC 2019 April 01.

Published in final edited form as:

J Biomed Mater Res A. 2018 April ; 106(4): 865–875. doi:10.1002/jbm.a.36323.

3D extrusion bioprinting of single- and double-network hydrogels containing dynamic covalent crosslinks

Leo L. Wang[1], **Christopher B. Highley**[1], **Yi-Cheun Yeh**[1], **Jonathan H. Galarraga**[1], **Selen Uman**[1], and **Jason A. Burdick**[1,*]

[1]Department of Bioengineering, University of Pennsylvania, Philadelphia, PA

Abstract

The fabrication of three-dimensional (3D) scaffolds is indispensable to tissue engineering and 3D printing is emerging as an important approach towards this. Hydrogels are often used as inks in extrusion-based 3D printing, including with encapsulated cells; however, numerous challenging requirements exist, including appropriate viscosity, the ability to stabilize after extrusion, and cytocompatibility. Here, we present a shear-thinning and self-healing hydrogel crosslinked through dynamic covalent chemistry for 3D bioprinting. Specifically, hyaluronic acid was modified with either hydrazide or aldehyde groups and mixed to form hydrogels containing a dynamic hydrazone bond. Due to their shear-thinning and self-healing properties, the hydrogels could be extruded for 3D printing of structures with high shape fidelity, stability to relaxation, and cytocompatibility with encapsulated fibroblasts (>80% viability). Forces for extrusion and filament sizes were dependent on parameters such as material concentration and needle gauge. To increase scaffold functionality, a second photocrosslinkable interpenetrating network was included that was used for orthogonal photostiffening and photopatterning through a thiol-ene reaction. Photostiffening increased the scaffold's modulus (~300%) while significantly decreasing erosion (~70%), whereas photopatterning allowed for spatial modification of scaffolds with dyes. Overall, this work introduces a simple approach to both fabricate and modify 3D printed scaffolds.

Keywords

3D printing; hydrogel; injectable; dynamic covalent chemistry; hydrazone

Introduction

Three-dimensional (3D) scaffolds have critical roles in tissue engineering and as in vitro models of tissues for drug testing.[(1)–(3)] Towards this, additive manufacturing (e.g., extrusion-based 3D printing) approaches allow for the fabrication of complex architectures with tunable properties using various biomaterials as bioinks. The printing of hydrogel-based scaffolds is attractive, as they offer cellular environments that can mimic those found in vivo, where features such as high water content and mechanics are similar to the natural extracellular matrix.[(4)–(6)] Hydrogels can also be further modified to permit and control cell

[*]**Corresponding Author:** Jason A. Burdick, Ph.D., Professor of Bioengineering, Department of Bioengineering, University of Pennsylvania, 240 Skirkanich Hall, 210 S. 33rd Street, Philadelphia, PA 19104, burdick2@seas.upenn.edu.

Author Manuscript Author Manuscript Author Manuscript Author Manuscript

interactions, such as phenotype, motility, and fate. Both natural and synthetic polymers have been used in this capacity, including but not limited to alginate,[7] gelatin,[8] fibrin,[9] collagen,[10] chitosan,[11] agarose,[12] and hyaluronic acid.[13],[14] The combination of these materials with cells or other bioactive molecules facilitates use in various biomedical applications.

In extrusion-based 3D printing of hydrogels, there are various design considerations. First, the material needs to be of sufficiently low viscosity to permit extrusion. However, upon deposition, viscosity must be either high enough to limit material dispersion or the material must undergo a rapid sol-gel transition to form a stable hydrogel. The mechanical properties of the hydrogel must also allow it to maintain its shape over time, including with the culture of cells. Whereas material properties can be tuned to achieve such criteria, it may come at the expense of cell viability. For example, biomaterials with high viscosity may introduce damaging shear stresses to cells during extrusion and cell viability is often improved in more loosely crosslinked hydrogels that permit the diffusion of nutrients and wastes.[6],[15]–[19] Thus, meeting these specific criteria is a major hurdle in the development of new hydrogel bioinks.

Shear-thinning and self-healing hydrogels based on physical crosslinking mechanisms have been explored as bioinks.[13],[14] Shear-thinning hydrogels flow during the application of mechanical force during extrusion by breaking apart physical crosslinks, which may then self-heal upon cessation of this force with deposition. Physically-crosslinked hydrogels can be printed without secondary crosslinking steps,[20] or secondary crosslinking may be needed to stabilize the printed structures to prevent relaxation over time.[14] Pre-crosslinking of covalent hydrogels can also be used to improve viscosity for printing, but secondary crosslinking steps are still necessary to obtain robust properties.[21] In either case, care should be taken to ensure that secondary crosslinking does not decrease cell viability or restrict desired cell behavior.[15]

Towards a new approach for bioink design, we explore here the use of dynamic covalent bonds for hydrogel formation. Dynamic covalent chemistries form covalent bonds that have significantly higher strengths than physical bonds, but are also reversible and in constant equilibrium between the bound and unbound state.[22]–[24] The use of these covalently adaptable bonds in cell-laden hydrogels is still relatively new, but they may have the added advantage of allowing cells to spread or move within the network as the local bonds rearrange, which is not possible with stable covalent crosslinks.[25] The dynamic behavior of various bonds has been reported, including acetals, alkoxyamines, borate esters, Diels-Alder cycloadditions, olefins, oximes, imines, and hydrazones.[24]

Here, we employed hydrazone chemistry in hyaluronic acid hydrogels, adapting from previously established chemistries that have allowed such hydrogels to be used in various biomedical applications.[26]–[28] The hydrazone bond is a unique dynamic covalent bond that is formed between an electron-dense, nucleophilic hydrazide (R-$NHNH_2$) and an electron-deficient, electrophilic aldehyde (R-CHO). Hydrazone crosslinked hydrogels and imine variants of the hydrazone bond have previously been explored for their injectable, shear-thinning and self-healing properties.[29]–[32] They have further been shown to protect cells

Author Manuscript Author Manuscript Author Manuscript Author Manuscript

during extrusion through a needle, adding to the advantages of using this system for 3D printing.[29] We hypothesized that hydrogels assembled through dynamic covalent crosslinking between hydrazide and aldehyde groups were shear-thinning and self-healing and would allow for extrusion for application in 3D bioprinting.

Materials and Methods

Materials

Hyaluronic acid (HA, MW = 400 kDa, 74 kDa) was purchased from LifeCore (Chaska, MN). All other reagents were purchased from Sigma-Aldrich (St. Louis, MO) unless specified otherwise.

HA-HYD synthesis and characterization

HA (74 kDa, 1 g) and adipic acid dihydrazide (~13 g, >60× molar excess) were dissolved in 200 mL dH_2O. 1-Ethyl-3-(3-dimethylaminopropyl)carbodiimide (EDC, 1.55 g, 10 mmol) and hydroxybenzotriazole (HOBt, 1.53 g, 10 mmol) were sere separately dissolved in a DMSO/dH_2O mixture (1:1) and added dropwise to the HA solution. pH was adjusted to 6.8 every 30 minutes for 4 hours, followed by reaction for 24 hours. The solution was dialyzed against dH_2O (3500 MWCO) for 3 days after which products were precipitated in cold acetone and dialyzed again for a week. Products were lyophilized and stored under nitrogen at −20°C for use. HA-HYD was characterized by ^1H NMR (DMX 360, Bruker, Billerica, MA) and was found to have a hydrazide modification of approximately 30% of disaccharide repeat units.

HA-ALD synthesis and characterization

HA (400 kDa, 200 mg) and sodium periodate (103 mg, 1:1 periodate/HA molar ratio) was dissolved in 20 mL dH_2O. The reaction was stirred for 2 hours in the dark and subsequently quenched in 2 mL ethylene glycol. The solution was then dialyzed for 5 days against dH_2O (14000 MWCO) and lyophilized. HA-ALD was stored under nitrogen at −20°C until use. To quantify aldehyde modification, HA-ALD was dissolved at 2 wt% and subsequent reacted with tert-Butyl carbazate (t-Bc, 1% in trichloroacetic acid) in dH_2O overnight as previously described.[33],[34] The next day, HA-ALD/t-BC and t-BC standards were reacted with 2,4,6-trinitrobenzenesulfonic acid (TNBS, 6 mM in 0.1 M sodium tetraborate, pH 8) for 1 hour. Samples were then reacted with 0.5 N hydrochloric acid and absorbance was measured at 340 nm on a microplate reader (Tecon).

Hydrogel assembly and syringe loading

HA-HYD and HA-ALD were dissolved separately in phosphate buffered saline (PBS) at desired concentrations and mixed for hydrogel formation with equal mass ratios of HA-HYD and HA-ALD. To load into syringes, polymers were manually mixed in syringe barrels and subsequently centrifuged to remove air bubbles. Hydrogels were allowed to form for a minimum of 2 hours in 37°C prior to use.

Author Manuscript Author Manuscript Author Manuscript Author Manuscript

Dynamic mechanical analysis (DMA)

Hydrogels (50 μL at 1.5, 3, 5 wt%) were formed in 4.7 mm diameter cylindrical molds. Compression testing was performed (TA Instruments, Q800) to evaluate the Young's modulus, failure stress, and failure strain. Hydrogels were secured within a fluid cup via a 0.01 N pre-load and subsequently compressed until failure at a rate of 0.5 N min^{-1}; moduli were evaluated as the slope from 10–20% strain. To assess the ability of hydrogels to self-heal, hydrogels were cut medially, resulting in half-cylinders. These half-cylinders were then placed into contact again and allowed to undergo self-healing over 30 minutes. Compression testing was then performed as described above to assess the Young's modulus, failure stress, and failure strain of samples after cutting and healing. The self-healing efficiency was quantified as failure stress of the cut and healed hydrogel (S_H) normalized to the failure stress of hydrogels tested without cutting (S_I).

Shear oscillatory rheometry

Measurements were performed using an AR2000 stress-controlled rheometer (TA Instruments) fitted with a 20 mm diameter cone and plate geometry, 59 min 42 s cone angle, and 27 μm gap. Rheological properties were examined by time sweeps (1.0 Hz; 0.5% strain). For shear recovery experiments, high 250% strain was applied with recovery at 0.5% strain, each at 1 Hz. To evaluate shear-thinning, material responses to shear were examined in continuous flow experiments with a linearly ramped shear rate from 1 to 100 s^{-1}. To measure photocuring of double-networks, UV was applied (10 mW/cm^2) using an Exfo Omnicure S1000 lamp with a 320−390 nm filter for 5 minutes via a UV-curing stage during oscillatory time sweeps (1.0 Hz, 0.5% strain).

Hydrogel erosion

Custom fabricated agarose molds in microcentrifuge tubes were used to contain 30 μL hydrogels with a 5 mm diameter and 6 mm depression. Hydrogels were covered in 500 μL PBS and allowed to erode at 37°C. At indicated timepoints, buffer was removed and replaced with fresh PBS. HA concentrations in releasates were quantified using a uronic acid assay.[35],[36] Briefly, 30 μL of buffer from each timepoint was added to a sodium tetraborate decahydrate solution in sulfuric acid (25 mM in H_2SO_4) and heated to 100°C for 10 minutes. 50 μl of carbazole (0.125% in ethanol) was added and solutions were heated to 100°C for 15 minutes. Solution absorbances were measured at 530 nm on a microplate reader. Serial dilutions of HA starting from 4 mg/mL were used to create a standard curve.

Cell encapsulation, viability, and activity assays

All macromers were sterilized under UV irradiation prior to use. NIH 3T3 fibroblasts grown in Dulbecco's Modified Eagle's medium (DMEM) supplemented with 10% fetal bovine serum and 1% penicillin/streptomycin were washed, trypsinized (0.05%), centrifuged, and resuspended in HA-HYD solutions toward a final concentration of 2×10^6/mL of hydrogel. HA-ALD solution was added to the HA-HYD cell suspension. Macromers were subsequently mixed and manually transferred to a 1 mL BD syringe to form hydrogels. For viability assays, flow rate was varied on a syringe pump (KD Scientific). Following printing, cells were stained with calcein AM/ethidium homodimer Live/Dead solution

Author Manuscript Author Manuscript Author Manuscript Author Manuscript

(ThermoFisher) according to manufacturer's instructions. For metabolic activity assays, hydrogels were printed into custom agarose wells as previously described.[37] Media was added above cells and changed every two days. At indicated timepoints, alamarBlue solution (10% in 3T3 media) was added for 4 hours, collected, and frozen. Quantification at each time point was performed on a microplate reader (Tecon) at an absorbance of 530 nm and emission of 590 nm on a microplate reader, and values were normalized to readings at D1 for each sample.

Force measurements, lattice construction and stability

Following hydrogel loading into syringes, syringes were placed into an Instron 5848 mechanical testing machine using a 50 N load cell under tensile extension mode to assess required forces to maintain a flow rate of 2 mL/hour. Printing was performed using a stepper motor-driven piston-based nozzle suitable for extrusion on a commercial 3D FDM printer (Revolution XL, Quintessential Universal Building Device) as previously described.[14],[38] Standard software was used to generate G-code (Slic3r) based on 3D computer-aided design (CAD) models (AutoCAD) and to control hardware (Repetier). Hydrogels were extruded at a moving speed of 40 mm/s. For fluorescent visualization of filaments, Rhodamine B isothiocyanate-dextran was mixed with macromers prior to use. Lattices were incubated in PBS at 37°C and imaged at indicated timepoints. For viability studies, printed structures were assessed for Live/Dead or activity as described above.

Double network formation and 3D printing

Nor-HA was synthesized as previously described from the tert-butyl ammonium salt of HA for a modification of 60% of disaccharide units on HA.[39] HA-HYD and HA-ALD were each dissolved in the dark with Nor-HA in PBS containing 4-(2-hydroxyethoxy)phenyl-(2-propyl)ketone (I2959, 0.05%) and pentaerythritol tetramercaptoacetate (PETMA) to theoretically consume 50% of free norbornenes. The two individual HA-HYD and HA-ALD solutions were mixed and vortexed for 1 min, and then transferred to a syringe for 3D printing. A 3D disc structure was printed from a respective 3D CAD model. The materials were loaded into syringes and printed with 25G needles. After printing, the structure was photocrosslinked with UV irradiation (365nm, 10 mW/cm^2, 2 mins). For erosion studies, filaments (100 μL) were extruded into 24-well plates and incubated in 1 mL PBS as described above.

Photopatterning of double networks

A fluorescent, thiolated peptide with the sequence GCKKG-rhodamine was synthesized by solid phase peptide synthesis (Protein Technologies) using glycinol 2-chlorotrityl resin and fluorenylmethyloxycarbonyl chloride-protected amino acids that were then reacted with the free acid of rhodamine. Printed and photostiffened hydrogel discs after printing were subsequently patterned as previously described.[39] In short, hydrogels were incubated with the thiolated rhodamine peptide (5 μM), I2959 (0.05%) and bovine serum albumin (1%) in PBS for 1 hour at room temperature. Hydrogels were then covered with a CAD drawn photomask (CAD/Art Services, Inc) and irradiated under UV (365nm, 10 mW/cm^2, 10 mins). Following UV administration, hydrogels were subsequently washed five times in PBS

Author Manuscript Author Manuscript Author Manuscript Author Manuscript

to remove unbound rhodamine, and an Olympus BX51 microscope (B&B Microscopes Limited) was used to image the patterns.

Statistical Analysis

All statistics were performed using Graphpad Prism 7. All data are reported as mean ± standard deviation and performed at a minimum in triplicate. Comparisons between two groups were performed by Students t-test with two-tailed criteria and significance determined at $p<0.05$. For comparison between multiple groups, significance was determined by one-way ANOVA with post hoc testing, or by two-way ANOVA when comparing effects of multiple independent variables. Bonferroni correction was used to account for multiple comparisons with $\alpha=0.05$.

Results and Discussion

Macromer synthesis, hydrogel formation, and mechanical properties

Hyaluronic acid (HA) was modified with hydrazides (HA-HYD) via amidation between adipic acid dihydrazide and carboxyl groups of HA or with aldehydes (HA-ALD) through oxidation with sodium periodate (Figure 1A). Synthesis of HA-HYD led to ~30% of modification disaccharide repeats with hydrazides (Supplement Figure 1). Synthesis of HA-ALD led to ~20% modification of disaccharide repeats with aldehydes (Figure S2A). Because the oxidation process to synthesize HA-ALD also hydrolyzes HA polymer chains, gas permeation chromatography (GPC) was used to measure the molecular weight of HA-ALD. The synthesized product was ~21 kDa, suggesting a large reduction in size during oxidation (Figure S2B). HA-HYD and HA-ALD were formed into hydrogels by mixing the two dissolved macromers manually, with gelation demonstrated by a qualitatively turning solutions to the side. Whereas HA-HYD and HA-ALD macromers alone rapidly flowed following turning to the side, the mixture of the two formed a solid hydrogel that did not flow after being turned to the side, both immediately after mixing and for up to two months (Figure 1B). This demonstrates a stable network that is resistant to flow with dynamic covalent crosslinks. In contrast, dynamic physical crosslinks often lead to hydrogel relaxation over the time course of minutes to hours.[14],[40] This may be attributed to the greater bond strength of the dynamic covalent bond compared to physical ones, and the equilibrium of the hydrazone bond chemistry which has been shown to strongly favor the bonded state.[25]

Using shear oscillatory rheometry, the kinetics of hydrogel formation was monitored at 3 concentrations (1.5, 3, 5 wt%) and a mass ratio of 1:1 of HA-HYD and HA-ALD, which corresponded to a 1.2:1 molar ratio of HYD to ALD (Figure 1C, Figure S3A–C, S3E). By increasing the macromer concentrations, the rates of gelation and the ultimate storage (G') and loss (G") moduli were altered. At 1.5 wt%, hydrogels formed slowly and reached an ultimate G' of ~500 Pa. By increasing to 3 and 5 wt%, hydrogels formed more quickly and reached G' of ~2000 and ~6000 Pa, respectively (Figure 1D). Of note, while rheometry provided relative measurements of the kinetics of gelation, manual mixing led to more rapid qualitative gelation. Further, we also varied the ratio of HA-HYD to HA-ALD, but found that changes in either direction lowered the overall hydrogel mechanics (Figure S3D). At the

Author Manuscript Author Manuscript Author Manuscript Author Manuscript

formulations investigated, erosion was also dependent on concentration, where 1.5 wt% hydrogels eroded ~70% by two weeks, 3 wt% eroded ~30%, and 5 wt% eroded ~20% (Figure 1E). Taken together, the mechanical properties of these hydrogels were shown to be tunable by controlling the macromer concentration in hydrogels, increasing properties through additional HA entanglements and hydrazone crosslink density. Increasing concentrations also affected the rates at which these macromers self-assembled into a hydrogel and the rates at which hydrogels eroded in buffer. Of note, high erosion rates were observed at later timepoints (1–2 weeks) for hydrogels at low concentrations (1.5 wt%). Thus, while the dynamic covalent bond may confer mechanical stability to relaxation, it is in a dynamic equilibrium with the unbound form, leading to erosion of macromers when hydrogels were incubated in buffer.

Injectability, shear-thinning and self-healing of hydrogels

After hydrogel formation and initial mechanical characterization, we investigated the shear-thinning and self-healing capacity of these hydrogels. Using shear oscillatory rheometry, we observed shear yielding from a strain sweep, where hydrogels at three different concentrations yielded at ~200% strain (Figure S4A). Moreover, increasing the shear rate led to decreased material viscosity, demonstrating shear-thinning (Figure 2A) and corroborating previous reports that demonstrated the shear-thinning ability of hydrogels assembled through hydrazone bonds.[29] Recognizing the ability for these hydrogels to undergo shear-thinning, we demonstrated qualitatively that the hydrogels could be ejected from a 27Gx1/2” insulin syringe (Figure 2B). To assess self-healing, hydrogels were formed into cylindrical discs and mixed with red and blue dyes. Separated red and blue discs were then cut in half and recombined with half of another disc with a different color. After 10 minutes, there was clear healing at the interface, and no separation of the discs when placed in PBS (Figure 2C). The healed hydrogel also could not be pulled apart manually (Figure 2D). Strain cycling on shear-oscillatory rheometry was also used to evaluate the hydrogels at low strain (0.5%) and in response to high, deforming strain (250%). Here, all formulations tested demonstrated a rapid decline in G’ upon application of high strain and rapid recovery upon cessation of this strain, demonstrating again the self-healing capacity of these materials (Figure 2E). In a syringe, the shear-thinning property of these hydrogels may manifest more as a shear-banding effect, where the intense shear experienced around the edges of the hydrogel permits material flow through a contribution from the disassembly of hydrazone bonds. However, there may be a component of brittle failure that occurs as well to permit extrusion of these materials through a syringe that actually leads to fracture-like behaviors; in these situations, macromers themselves may be broken or forced into high energy configurations to allow the hydrogel to pass through the needle. The self-healing properties of these materials are thus paramount to their ability to be extruded, as bonds that break at fractured interfaces are able to slowly re-heal following hydrogel extrusion.

Finally, the Young’s modulus and healing efficiency of these hydrogels was assessed using DMA (Figure 2F). Healing efficiency was defined as the ratio between the failure stress of hydrogel discs after cutting in half and re-healing for 30 minutes (S_H) and the failure stress of hydrogel discs that were not cut in half (S_I). This was adapted from previously described protocols for self-healing.[31],[32],[41] As the concentration of the hydrogels increased, the

Author Manuscript Author Manuscript Author Manuscript Author Manuscript

Young's modulus increased from ~3 kPa at 1.5 wt% to ~10 kPa at 3 wt% to ~15–20 kPa at 5 wt%. Interestingly, the healing efficiency of hydrogels was highest at 1.5 wt%, achieving a healing efficiency of almost 100% where failure stress was nearly restored (Figure S4B). Higher concentrations also healed qualitatively, but only reached a healing efficiency of ~50%. All formulations investigated reached similar failure strains before and after healing (Figure S4C). Longer healing times (>30 minutes) may thus be necessary to achieve complete healing of higher concentration hydrogels (3, 5 wt%). Because low concentration hydrogels (1.5 wt%) exhibited the best healing, we hypothesize that lower crosslink densities may require fewer bonds to re-form to confer mechanical strength to compression after healing. Similarly, because hydrazone bond breakage is a hydrolytic reaction, the higher water content in lower concentration (1.5 wt%) hydrogels may facilitate additional bond rearrangements. There may also be greater mobility of macromers at lower concentrations, allowing unbound aldehydes to find hydrazides for reaction. At higher concentrations, healing may require longer times due to larger rearrangements that may be necessary to fully pair up crosslinks; such rearrangements may be prohibited by dense entanglements and other crosslinks in the network.

Cell encapsulation and viability in hydrogels

As a step towards applying the hydrogels to bioprinting, we encapsulated cells within the hydrogels and investigated their viability for up to 14 days. Specifically, 3T3 fibroblasts were mixed with the macromer components during the gelation. Calcein AM and ethidium homodimer were used to measure live and dead cells, respectively, demonstrating high cell viability 1 day after encapsulation based on imaging (Figure 3A). Quantification of live cells relative to total cells 1 day after encapsulation demonstrated ~80–90% viability for cells in hydrogels across all concentrations tested (Figure 3B). For long-term viability analysis, encapsulated cells in hydrogels were placed into agarose well molds and the metabolic activity was measured by addition of alamarBlue, an indicator of cellular activity (Figure S5). The metabolic activity increased for all hydrogel concentrations, but increased fastest in hydrogels at 1.5 wt% and slowest at 5 wt% (Figure 3C). Qualitatively, the alamarBlue reagents did not change the color of hydrogels without cells but changed the color of hydrogels with cells to an intense pink (Figure S5) to demonstrate cell activity. This data supports previous reports that low density polymer environments may be more conducive to cell growth and viability[17] and suggests that that decreased polymer-polymer interactions may be more favorable for cell viability. There may also be a contribution of the hydrazone bond that facilities cell activity as it has previously been shown that dynamic bonds can be rearranged to permit cell spreading.[25] This data also corroborates previous reports that demonstrated high cell viability in both HA hydrogels and hydrazone-crosslinked hydrogels.[14],[25],[29],[42]

Extrusion-printing of hydrogel filaments

Towards extrusion-based 3D printing, we studied properties of extrusion by varying material and printing parameters. First, we measured force profiles of hydrogels (1.5, 3, 5 wt%) extruded through increasingly smaller needles (18, 23, 25G) at a fixed length (1/4") and at a constant extrusion rate (Figure 4A). At a fixed concentration, increasing the needle gauge increased the required force needed for extrusion but also led to small fluctuations in force

Author Manuscript Author Manuscript Author Manuscript Author Manuscript

over time that could indicate heterogeneity in the network and potentially alter filament uniformity (Figure S6A). Likewise, at a fixed needle gauge, the force required to extrude the hydrogels increased with increasing macromer concentration (Figure 4A, Figure S6B). As force requirements for extrusion changed, there was also more fluctuation in forces at 3 and 5 wt%; however, with the largest needle tested (18G) and using the lowest concentration (1.5 wt%) a stable force profile was observed (Figure S6C). When filaments were printed, the needle gauge had a direct impact on the filament diameter at 1.5 and 3 wt%, as higher needle gauges with smaller inner diameters yielded filaments with smaller diameters (Figure 4B). While 5 wt% hydrogels were printable into filaments at all needle gauges, filaments were fractured and inconsistent in size (Figure S6D).

Cell viability was also influenced by the printing parameters investigated, including 1.5 and 3 wt% hydrogels (as 5 wt% hydrogels did not lead to good filament fidelity they were not included in further studies), three needle gauges (18, 23, 25G), and two flow rates (0.5, 1 mL/hr). Whereas modest viability after extrusion (~70%) was achieved across all conditions tested, the best viability was achieved using the 1.5 wt% hydrogel and 18G needle (~90%) (Figure S6E). This formulation corresponded to the least force required for extrusion (Figure 4A), suggesting that the force directly impacts cell viability during printing, corroborating previous reports of the relationship between substrate stiffness and cell viability.[18] The dynamic covalent bonds here likely play an important role in protecting cells from experiencing shear during the extrusion process.[29] Recognizing that printing of 1.5 wt% hydrogels with an 18G needle led to the lowest forces and highest viability, we printed filaments of this composition with encapsulated rhodamine dextran for visualization (Figure 4C). We note that filaments could be printed with higher resolution with smaller needles (e.g. 23G, 25G), but these parameters would decrease cell viability. Printed filaments were smooth with high shape fidelity and did not relax during the printing process or for up to 30 minutes in either air and PBS, suggesting the potential for this formulation in fabricating 3D scaffolds (Figure 4D).

Printing of multilayer lattices

Towards the fabrication of multi-layered scaffolds, hydrogels at 1.5 wt% were formed and ejected through an 18G needle into a 3D, multi-layer lattice consisting of filaments spaced 3 mm apart (Figure 5A). A 4-layer lattice was fabricated that was stable both in air and PBS immediately after printing (Figure 5B), with minimal changes for up to 5 days (Figure 5C). In air, filaments were stable over time, changing minimally over the first two hours after printing and subsequently did not change in appearance or relax (Figure S7A, Figure S7B). Constructs were also stable in PBS immediately after immersion and for up to one week (Figure S7C), but did experience some swelling with time and filament diameters increased by ~170% (Figure S7D), which may be a result of the dynamic covalent bond that permits network rearrangements. For bioprinting, cells were encapsulated in hydrogels and printed (Figure 5D). High viability was observed (~85%), comparable to the viability of cells in hydrogels before printing (~95%) (Figure 5E). AlamarBlue was used to quantify metabolic activity, demonstrating increased activity over time in 3D printed constructs (Figure 5F) that did not differ from activity in non-printed constructs. These data suggest that viable cells can be 3D printed within hydrogels containing covalent bonds.

Author Manuscript Author Manuscript Author Manuscript Author Manuscript

Double-network hydrogels

As another approach to control printed hydrogel properties, the use of double-networks was investigated. Specifically, norbornene-modified HA (Nor-HA) was synthesized through an esterification reaction between a carboxylated norbornene and the hydroxyl group of HA (Figure 6A), leading to a norbornene modification of ~60% of HA disaccharide repeat units (Figure S8). Norbornenes react with thiols in response to ultraviolet light and photoinitiator to undergo a radical-initiated thiol-ene click reaction. Thus, the introduction of Nor-HA and crosslinker within the HA-HYD/HA-ALD hydrogels could be used to produce a double-network, where post-crosslinking of the Nor-HA network could confer additional long-term stability and improved mechanics. To test this, Nor-HA, HA-HYD, and HA-ALD were mixed in the presence of a PETMA crosslinker, a tetrathiol, and I2959 photoinitiator to form a double network (Figure 6B). Rheology showed that ultraviolet light increased hydrogel mechanics, where G' increased from ~500 Pa to ~5 kPa (Figure 6C).

The use of Nor-HA as a secondary network also provides reactivity to pattern other signals into 3D printed structures, such as thiolated molecules.[39] In this process, Nor-HA crosslinking is first used to photostiffen the hydrogels to increase the mechanics and then another reaction is used to pattern molecules, adding heterogeneity to 3D constructed architectures (Figure 7A). To demonstrate photostiffening, double network hydrogels were printed into 5 mm discs with ~50% of norbornenes consumed during crosslinking (Figure S9A). Without the secondary networks, discs had a Young's modulus of ~1 kPa and increased to ~3 kPa after photocuring. The failure stress before light exposure was ~10 kPa and increased to ~30 kPa following curing (Figure S9B), while failure strain was unaffected (Figure S9C). To evaluate the effect of the secondary network on filament erosion, networks were printed and subsequently photostiffened for analysis via uronic acid relase. The introduction of the secondary network significantly decreased filament erosion to ~20% after 2 weeks, as compared to ~70% for constructs that were not photocured (Figure 7D). We note that erosion profiles of printed filaments may differ from macroscopically-crosslinked hydrogels due to increased surface area. in Photocuring also led to filaments that were significantly more stable to swelling over time, as filament diameters were maintained with photocuring but continued to increase over 24 hours without UV curing (Figure 7E). For photopatterning, double network discs with ~50% of norbornenes consumed were incubated in a solution of thiolated rhodamine and I2959 and subsequently exposed to ultraviolet light under two different photomasks of line and dot patterns. Hydrogels were then washed to remove unbound dye and subsequently imaged for pattern visualization (Figure 7F). Taken together, these results demonstrate the additional heterogeneity in mechanics and biomolecule presentation that can be introduced into the system by incorporation of a secondary Nor-HA double network into hydrogels.

Conclusions

3D extrusion bioprinting of hydrogels continues to be an evolving field that necessitates evolving bioinks. We successfully printed HA hydrogels assembled through hydrazone bonds that possessed dynamic covalent chemistry, which permitted the shear-thinning and self-healing properties needed for extrusion and material deposition. Extrusion forces for

Author Manuscript Author Manuscript Author Manuscript Author Manuscript

printing were dependent on needle gauge and hydrogel concentration and encapsulated cell viability was high under optimal conditions. A double-network approach was taken, where a photocrosslinkable network was introduced throughout this original network. This permitted an increase in mechanics with light exposure and permitted patterning of dyes with light exposure through a mask. Printing of these networks may permit the fabrication of complex biological scaffolds with controlled heterogeneity in mechanics and biomolecule presentation across multiple length scales.[43] This can have major advantages to the field of tissue engineering, where we are currently limited by the biological complexity of engineered scaffolds.

Supplementary Material

Refer to Web version on PubMed Central for supplementary material.

Acknowledgments

The authors thank M. Davidson for assistance with confocal imaging. This work was made possible by financial support from the American Heart Association through an Established Investigator Award to J.A.B. and pre-doctoral fellowship to L.L.W., the National Institutes of Health (F30 HL134255), and a National Science Foundation Graduate Research Fellowship to J.H.G.

References

1. Loh QL, Choong C. Three-Dimensional Scaffolds for Tissue Engineering Applications: Role of Porosity and Pore Size. Tissue Eng Part B Rev. 2013; 19:485–502. [PubMed: 23672709]
2. Lee JM, Yeong WY. Design and Printing Strategies in 3D Bioprinting of Cell-Hydrogels: A Review. Adv Healthc Mater. 2016; 5:2856–65. [PubMed: 27767258]
3. Groll J, Boland T, Blunk T, Burdick JA, Cho D-W, Dalton PD, Derby B, Forgacs G, Li Q, Mironov VA, Moroni L, Nakamura M, Shu W, Takeuchi S, Vozzi G, Woodfield TBF, Xu T, Yoo JJ, Malda J. Biofabrication: reappraising the definition of an evolving field. Biofabrication. 2016; 8:13001.
4. Ozbolat IT, Hospodiuk M. Current advances and future perspectives in extrusion-based bioprinting. Biomaterials. 2016; 76:321–43. [PubMed: 26561931]
5. Tibbitt MW, Anseth KS. Hydrogels as extracellular matrix mimics for 3D cell culture. Biotechnol Bioeng. 2009; 103:655–63. [PubMed: 19472329]
6. Tirella A, De Maria C, Criscenti G, Vozzi G, Ahluwalia A. The PAM^2 system: a multilevel approach for fabrication of complex three-dimensional microstructures. Rapid Prototyp J. 2012; 18:299–307.
7. Khalil S, Sun W. Bioprinting Endothelial Cells With Alginate for 3D Tissue Constructs. J Biomech Eng. 2009; 131:111002. [PubMed: 20353253]
8. Kolesky DB, Truby RL, Gladman AS, Busbee TA, Homan KA, Lewis JA. 3D Bioprinting of Vascularized, Heterogeneous Cell-Laden Tissue Constructs. Adv Mater. 2014; 26:3124–30. [PubMed: 24550124]
9. Cui X, Boland T. Human microvasculature fabrication using thermal inkjet printing technology. Biomaterials. 2009; 30:6221–7. [PubMed: 19695697]
10. Rhee S, Puetzer JL, Mason BN, Reinhart-King CA, Bonassar LJ. 3D Bioprinting of Spatially Heterogeneous Collagen Constructs for Cartilage Tissue Engineering. ACS Biomater Sci Eng. 2016; 2:1800–5.
11. Wu Q, Maire M, Lerouge S, Therriault D, Heuzey M-C. 3D Printing of Microstructured and Stretchable Chitosan Hydrogel for Guided Cell Growth. Adv Biosyst. 2017; 1:1700058.
12. Fan R, Piou M, Darling E, Cormier D, Sun J, Wan J. Bio-printing cell-laden Matrigel–agarose constructs. J Biomater Appl. 2016; 31:684–92. [PubMed: 27638155]
13. Highley CB, Rodell CB, Burdick JA. Direct 3D Printing of Shear-Thinning Hydrogels into Self-Healing Hydrogels. Adv Mater. 2015; 27:5075–9. [PubMed: 26177925]

Author Manuscript Author Manuscript Author Manuscript Author Manuscript

14. Ouyang L, Highley CB, Rodell CB, Sun W, Burdick JA. 3D Printing of Shear-Thinning Hyaluronic Acid Hydrogels with Secondary Cross-Linking. ACS Biomater Sci Eng. 2016; 2:1743–51.
15. Malda J, Visser J, Melchels FP, Jüngst T, Hennink WE, Dhert WJA, Groll J, Hutmacher DW. 25th Anniversary Article: Engineering Hydrogels for Biofabrication. Adv Mater. 2013; 25:5011–28. [PubMed: 24038336]
16. Mazzoccoli JP, Feke DL, Baskaran H, Pintauro PN. Mechanical and cell viability properties of crosslinked low- And high-molecular weight poly(ethylene glycol) diacrylate blends. J Biomed Mater Res - Part A. 2010; 93:558–66.
17. DeForest CA, Anseth KS. Advances in Bioactive Hydrogels to Probe and Direct Cell Fate. Annu Rev Chem Biomol Eng. 2012; 3:421–44. [PubMed: 22524507]
18. Tirella A, Vozzi F, De Maria C, Vozzi G, Sandri T, Sassano D, Cognolato L, Ahluwalia A. Substrate stiffness influences high resolution printing of living cells with an ink-jet system. J Biosci Bioeng. 2011; 112:79–85. [PubMed: 21497548]
19. Tirella A, Vozzi F, Vozzi G, Ahluwalia A. PAM2 (Piston Assisted Microsyringe): A New Rapid Prototyping Technique for Biofabrication of Cell Incorporated Scaffolds. Tissue Eng Part C Methods. 2011; 17:229–37. [PubMed: 20799910]
20. Schacht K, Jüngst T, Schweinlin M, Ewald A, Groll J, Scheibel T. Biofabrication of cell-loaded 3D spider silk constructs. Angew Chemie. 2015; 54:2816–20.
21. Rutz AL, Hyland KE, Jakus AE, Burghardt WR, Shah RN. A Multimaterial Bioink Method for 3D Printing Tunable, Cell-Compatible Hydrogels. Adv Mater. 2015; 27:1607–14. [PubMed: 25641220]
22. Rosales AM, Anseth KS. The design of reversible hydrogels to capture extracellular matrix dynamics. Nat Rev Mater. 2016; 1:15012. [PubMed: 29214058]
23. Rowan SJ, Cantrill SJ, Cousins GRL, Sanders JKM, Stoddart JF. Dynamic Covalent Chemistry. Angew Chemie. 2002; 41:898–952.
24. Jin Y, Yu C, Denman RJ, Zhang W. Recent advances in dynamic covalent chemistry. Chem Soc Rev. 2013; 42:6634. [PubMed: 23749182]
25. McKinnon DD, Domaille DW, Cha JN, Anseth KS. Biophysically Defined and Cytocompatible Covalently Adaptable Networks as Viscoelastic 3D Cell Culture Systems. Adv Mater. 2014; 26:865–72. [PubMed: 24127293]
26. Ito T, Yeo Y, Highley CB, Bellas E, Benitez CA, Kohane DS. The prevention of peritoneal adhesions by in situ cross-linking hydrogels of hyaluronic acid and cellulose derivatives. Biomaterials. 2007; 28:975–83. [PubMed: 17109954]
27. Yeo Y, Highley CB, Bellas E, Ito T, Marini R, Langer R, Kohane DS. In situ cross-linkable hyaluronic acid hydrogels prevent post-operative abdominal adhesions in a rabbit model. Biomaterials. 2006; 27:4698–705. [PubMed: 16750564]
28. Yeo Y, Ito T, Bellas E, Highley CB, Marini R, Kohane DS. In Situ Cross-linkable Hyaluronan Hydrogels Containing Polymeric Nanoparticles for Preventing Postsurgical Adhesions. Ann Surg. 2007; 245:819–24. [PubMed: 17457177]
29. Wang H, Zhu D, Paul A, Cai L, Enejder A, Yang F, Heilshorn SC. Covalently Adaptable Elastin-Like Protein-Hyaluronic Acid (ELP-HA) Hybrid Hydrogels with Secondary Thermoresponsive Crosslinking for Injectable Stem Cell Delivery. Adv Funct Mater. 2017; 27:1605609.
30. Chang R, Wang X, Li X, An H, Qin J. Self-Activated Healable Hydrogels with Reversible Temperature Responsiveness. ACS Appl Mater Interfaces. 2016; 8:25544–51. [PubMed: 27589014]
31. Huang W, Wang Y, Chen Y, Zhao Y, Zhang Q, Zheng X, Chen L, Zhang L. Strong and Rapidly Self-Healing Hydrogels: Potential Hemostatic Materials. Adv Healthc Mater. 2016; 5:2813–22. [PubMed: 27717239]
32. Wei Z, Yang JH, Liu ZQ, Xu F, Zhou JX, Zrínyi M, Osada Y, Chen YM. Novel Biocompatible Polysaccharide-Based Self-Healing Hydrogel. Adv Funct Mater. 2015; 25:1352–9.
33. Purcell BP, Lobb D, Charati MB, Dorsey SM, Wade RJ, Zellars KN, Doviak H, Pettaway S, Logdon CB, Shuman JA, Freels PD, Gorman JH, Gorman RC, Spinale FG, Burdick JA. Injectable and bioresponsive hydrogels for on-demand matrix metalloproteinase inhibition. Nat Mater. 2014; 13:653–61. [PubMed: 24681647]

Author Manuscript Author Manuscript Author Manuscript Author Manuscript

34. Su W-Y, Chen Y-C, Lin F-H. Injectable oxidized hyaluronic acid/adipic acid dihydrazide hydrogel for nucleus pulposus regeneration. Acta Biomater. 2010; 6:3044–55. [PubMed: 20193782]
35. Burdick JA, Chung C, Jia X, Randolph MA, Langer R. Controlled Degradation and Mechanical Behavior of Photopolymerized Hyaluronic Acid Networks. Biomacromolecules. 2005; 6:386–91. [PubMed: 15638543]
36. Bitter T, Muir H. A modified uronic acid carbazole reaction. Anal Biochem. 1962; 4:330–4. [PubMed: 13971270]
37. Loebel C, Rodell CB, Chen MH, Burdick JA. Shear-thinning and self-healing hydrogels as injectable therapeutics and for 3D-printing. Nat Protoc. 2017; 12:1521–41. [PubMed: 28683063]
38. Ouyang L, Highley CB, Sun W, Burdick JA. A Generalizable Strategy for the 3D Bioprinting of Hydrogels from Nonviscous Photo-crosslinkable Inks. Adv Mater. 2017; 29:1604983.
39. Gramlich WM, Kim IL, Burdick JA. Synthesis and orthogonal photopatterning of hyaluronic acid hydrogels with thiol-norbornene chemistry. Biomaterials. 2013; 34:9803–11. [PubMed: 24060422]
40. Rodell CB, Kaminski AL, Burdick JA. Rational design of network properties in guest-host assembled and shear-thinning hyaluronic acid hydrogels. Biomacromolecules. 2015; 14:4125–34.
41. Burattini S, Greenland BW, Chappell D, Colquhoun HM, Hayes W. Healable polymeric materials: a tutorial review. Chem Soc Rev. 2010; 39:1973. [PubMed: 20502798]
42. Rodell CB, Dusaj NN, Highley CB, Burdick JA. Injectable and Cytocompatible Tough Double-Network Hydrogels through Tandem Supramolecular and Covalent Crosslinking. Adv Mater. 2016; 28:8419–24. [PubMed: 27479881]
43. De Maria C, Vozzi G, Moroni L. Multimaterial, heterogeneous, and multicellular three-dimensional bioprinting. MRS Bull. 2017; 42:578–84.

Author Manuscript Author Manuscript Author Manuscript Author Manuscript

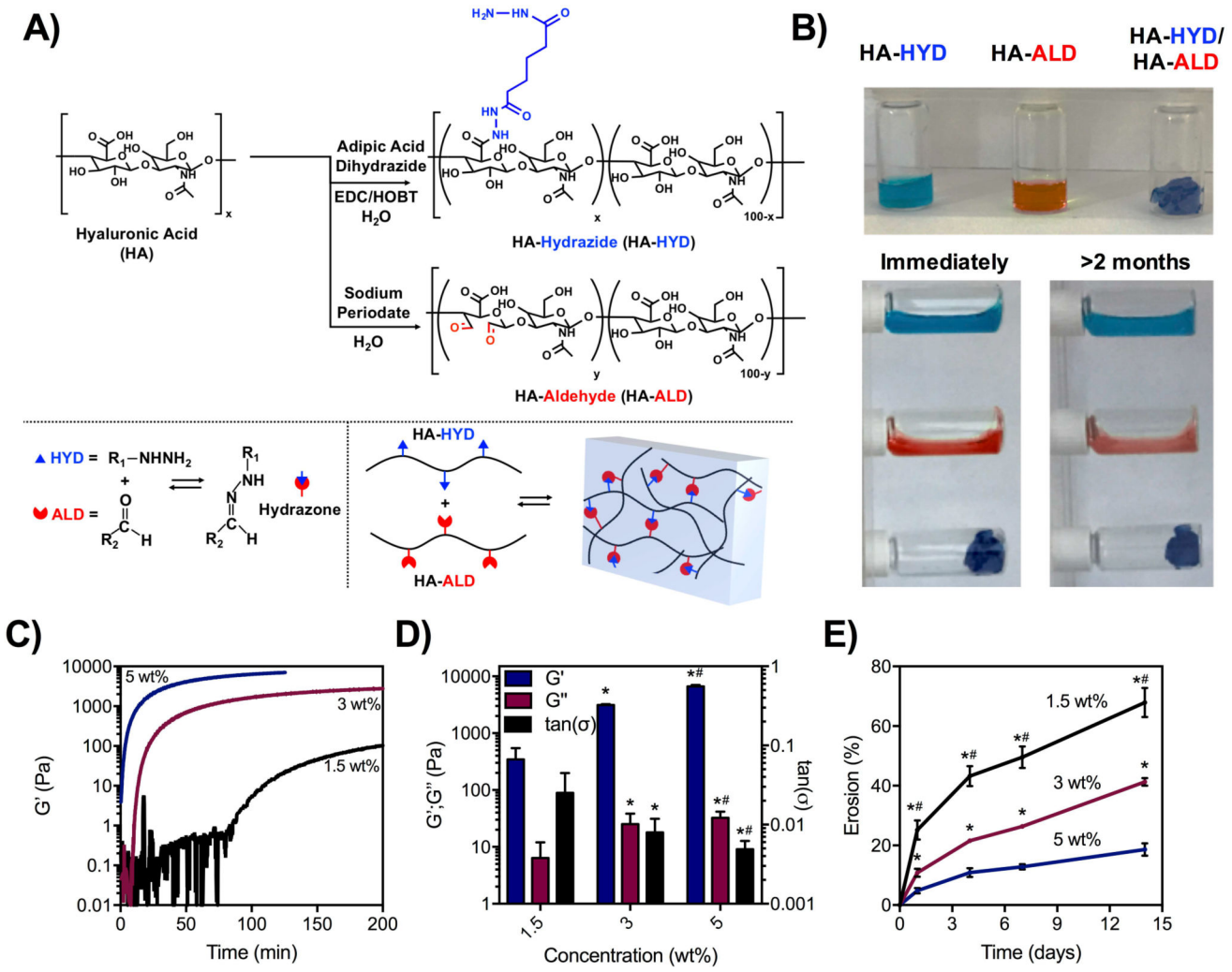

Figure 1. Modification of hyaluronic acid, hydrogel formation, and mechanical characterization

A) Synthesis schematic of hydrazide-modified HA (HA-HYD) and aldehyde-modified HA (HA-ALD) through an amidation reaction between the carboxyl group of HA and hydrazides of adipic acid dihydrazide and the oxidization of HA by sodium periodate, respectively. B) Stability of solutions of HA-HYD alone, HA-ALD alone, and after mixing (1.5 wt%) immediately after being placed on their side and after two months, demonstrating stable hydrogel formation when mixed. C) Time sweeps (1 Hz, 0.5% strain) and D) quantification of storage modulus (G'), loss modulus (G"), and tan(δ) of 1.5, 3, and 5 wt% hydrogels (1:1 mass ratio of HA-HYD:HA-ALD) on shear-oscillatory rheometry, demonstrating tunability in mechanics and gelation behavior with macromer concentration. *$p<0.05$ compared to 1.5 wt%, #$p<0.05$ compared to 3 wt%. E) Erosion of hydrogels at 37 °C by colorimetric measurements of uronic acid release over time of these same hydrogel compositions. *$p<0.05$ compared to 5 wt%, #$p<0.05$ compared to 3 wt%.

Author Manuscript Author Manuscript Author Manuscript Author Manuscript

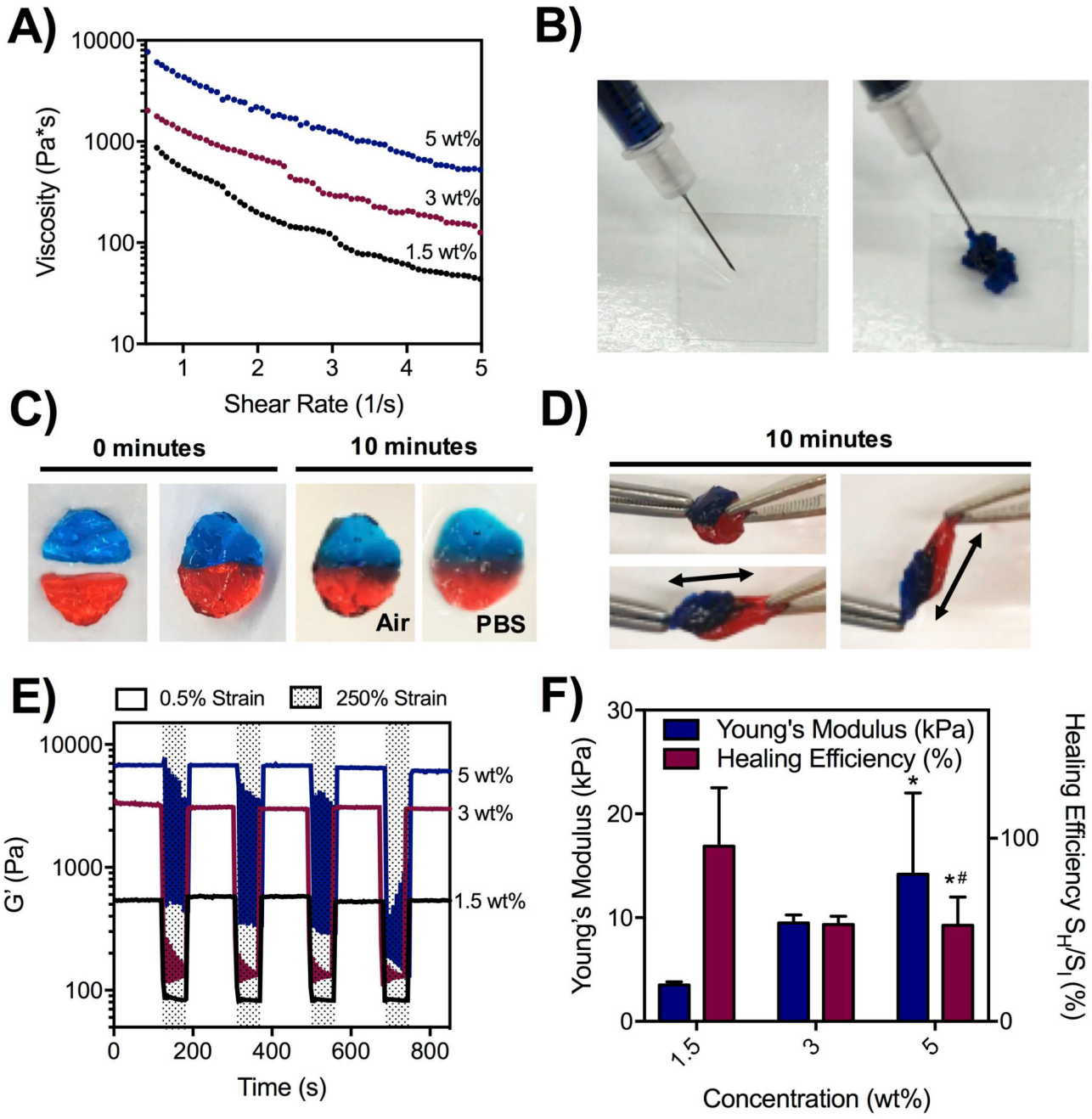

Figure 2. Injectability, shear-thinning, and self-healing of hydrogels

A) Shear-thinning of hydrogels measured with shear oscillatory rheometry, demonstrating decreasing viscosity with increasing shear-rates for 1.5, 3, and 5 wt% hydrogels. B) Ejection of hydrogels (1.5 wt%) from a 27Gx1/2" needle and syringe, demonstrating injectability. C) Self-healing of two dyed hydrogel discs (1.5 wt%) in air and PBS after 10 minutes. D) Manual stretching of healed hydrogel discs (1.5 wt%) after 10 minutes. E) Application of cyclic low (0.5%) and high (250%) strain on shear-oscillatory rheometry, demonstrating a rapid decrease in modulus in response to strain and a rapid recovery upon cessation of shear, applicable over multiple cycles of loading across 1.5, 3, and 5 wt% hydrogels. F) Dynamic

Author Manuscript Author Manuscript Author Manuscript Author Manuscript

mechanical analysis measurements of hydrogel Young's moduli, as well as healing efficiency – measured as the failure stress of hydrogels after cutting in half and 30 minutes of healing, normalized to the failure stress of hydrogels that were not cut – for 1.5, 3, and 5 wt% hydrogels.$^{*}p<0.05$ compared to 1.5 wt%,$^{\#}p<0.05$ compared to 3 wt%.

Author Manuscript Author Manuscript Author Manuscript Author Manuscript

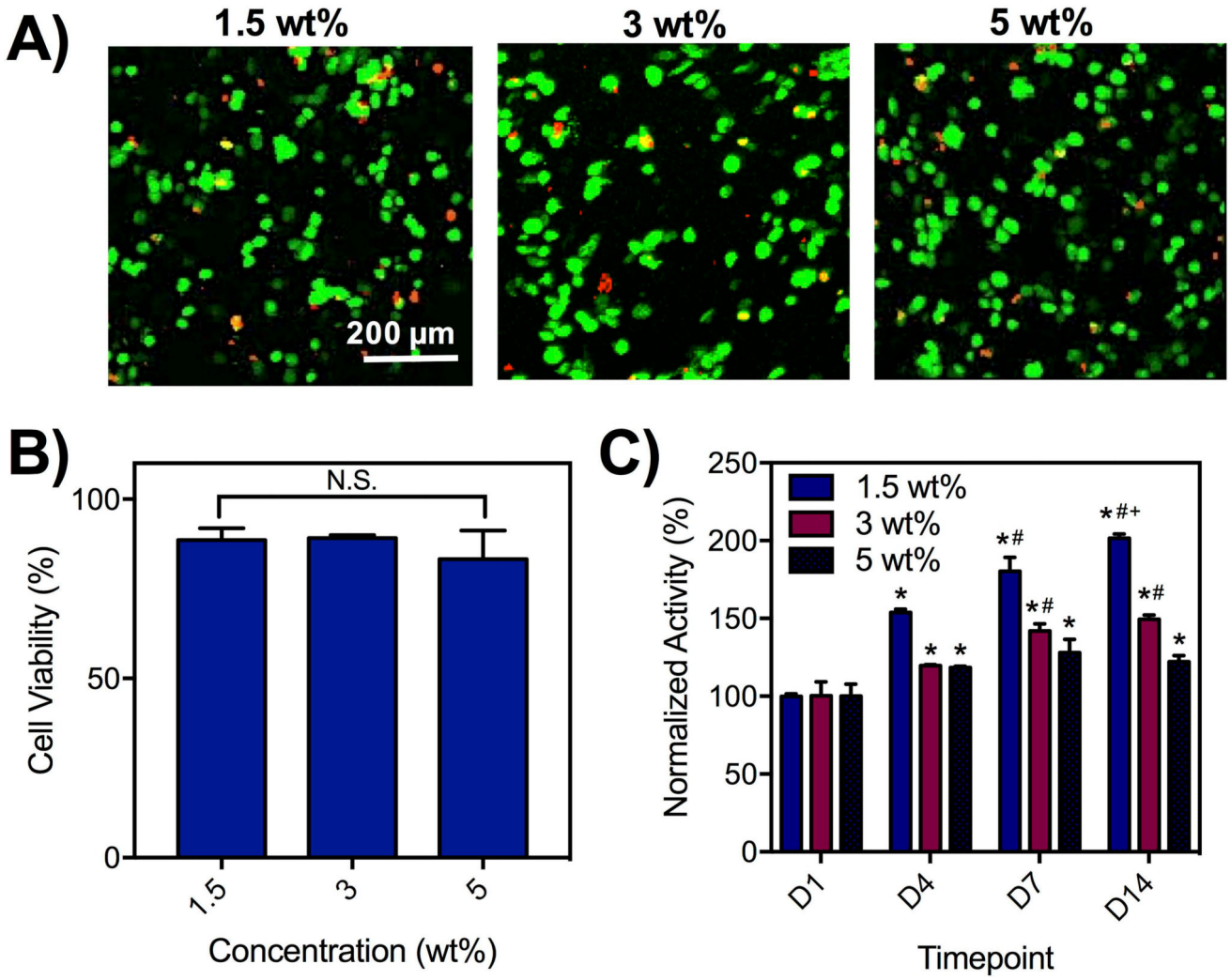

Figure 3. Cytocompatibility of hydrogels with encapsulated cells

A) Live/Dead staining and B) quantification of viability (% of live cells/total cells) of 3T3 fibroblasts (2×10^6/mL) encapsulated in hydrogels (1.5, 3, 5 wt%) after 1 day. N.S. = not significant between groups. C) AlamarBlue assessment of the activity of cells encapsulated in hydrogels (1.5, 3, 5 wt%), normalized to activity measurements after 1 day. $^{*}p<0.05$ compared to D1, $^{\#}p<0.05$ compared to D4, $^{+}p<0.05$ compared to D7.

Author Manuscript Author Manuscript Author Manuscript Author Manuscript

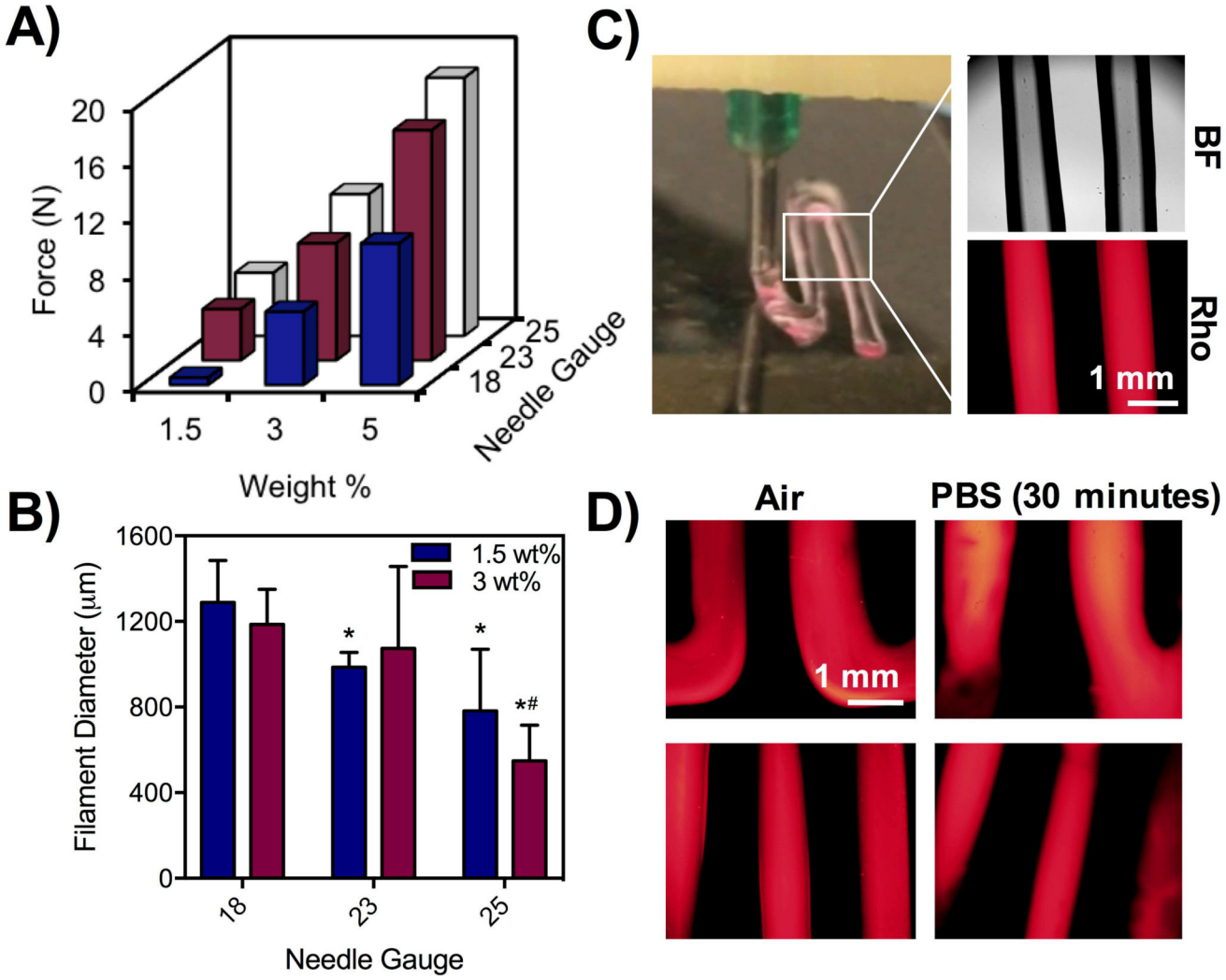

Figure 4. Effect of macromer concentration and needle gauge on force, filament printing, and viability

A) Force measurements from Instron testing of hydrogels at 1.5, 3, and 5 wt% and 18, 23, and 25G needles at a rate of 2 mm/min. B) Quantification of filament diameters from 1.5 and 3 wt% hydrogels using 18, 23, and 25G needles. Hydrogels were encapsulated with rhodamine-dextran for imaging and quantification of filament size.$^{*}p<0.05$ compared to 18G,$^{\#}p<0.05$ compared to 23G. C) Photo of printing with hydrogels containing rhodamine-dextran under bright field and fluorescent channels. D) Fluorescent images of filaments in air and in PBS after 30 minutes.

Author Manuscript Author Manuscript Author Manuscript Author Manuscript

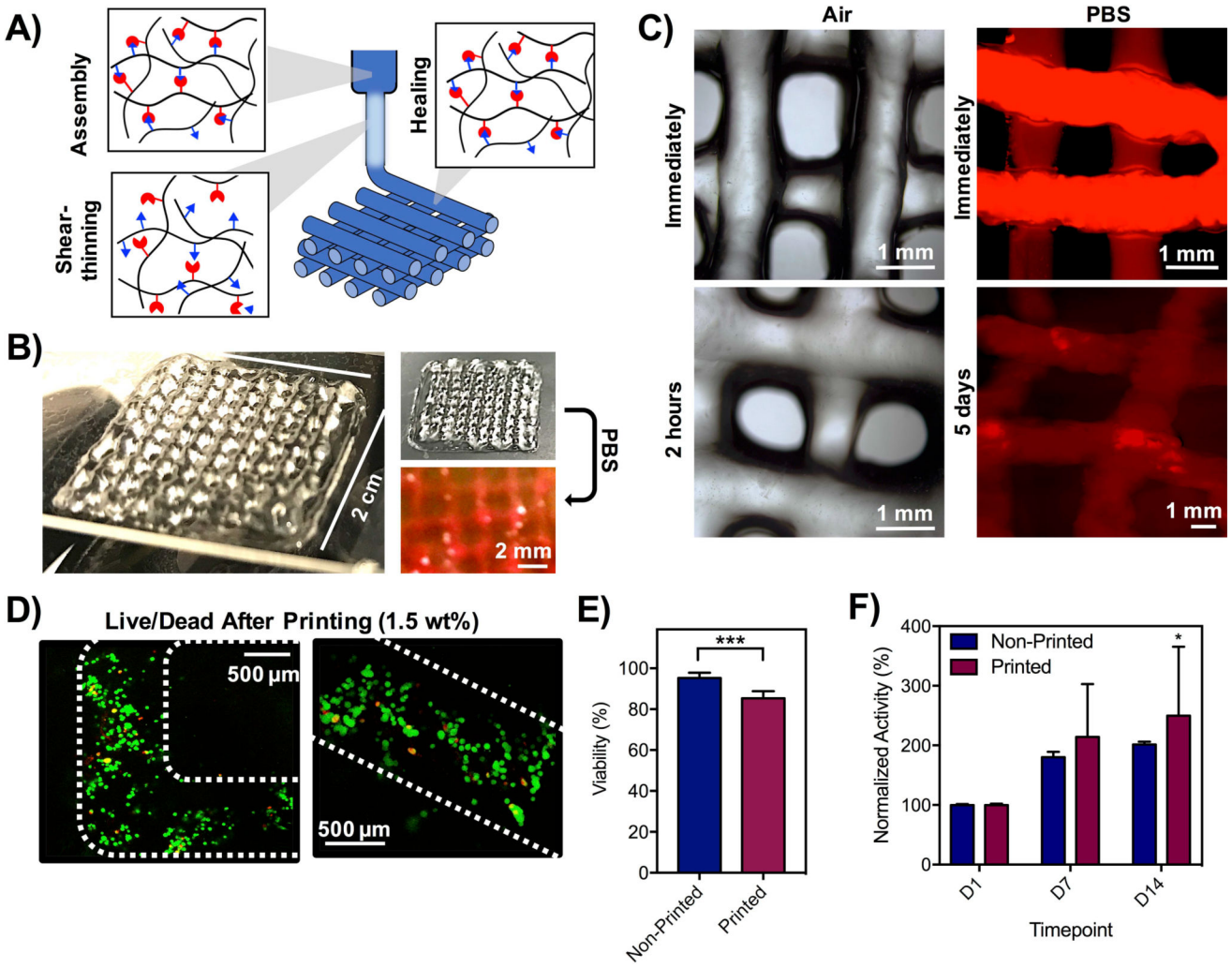

Figure 5. 3D printing of hydrogels into 3D, multilayer lattices

A) Schematic of shear-thinning and self-healing of hydrogels during printing, where hydrogels were formed in syringes, sheared through the extrusion process, and filaments stabilized by self-healing properties of hydrazone bonds. B) Photos of 4-layer lattices in air and in PBS. C) Images of lattices in air and in PBS (labeled with rhodamine-dextran). D) Live/Dead staining of cells in lattice filaments immediately after extrusion and E) quantification of cell viability before and after printing based on Live/Dead staining. ***p<0.001. F) Metabolic activity of cells in hydrogels before and after printing by alamarBlue measurements of activity. *p<0.05 compared to D1.

Author Manuscript Author Manuscript Author Manuscript Author Manuscript

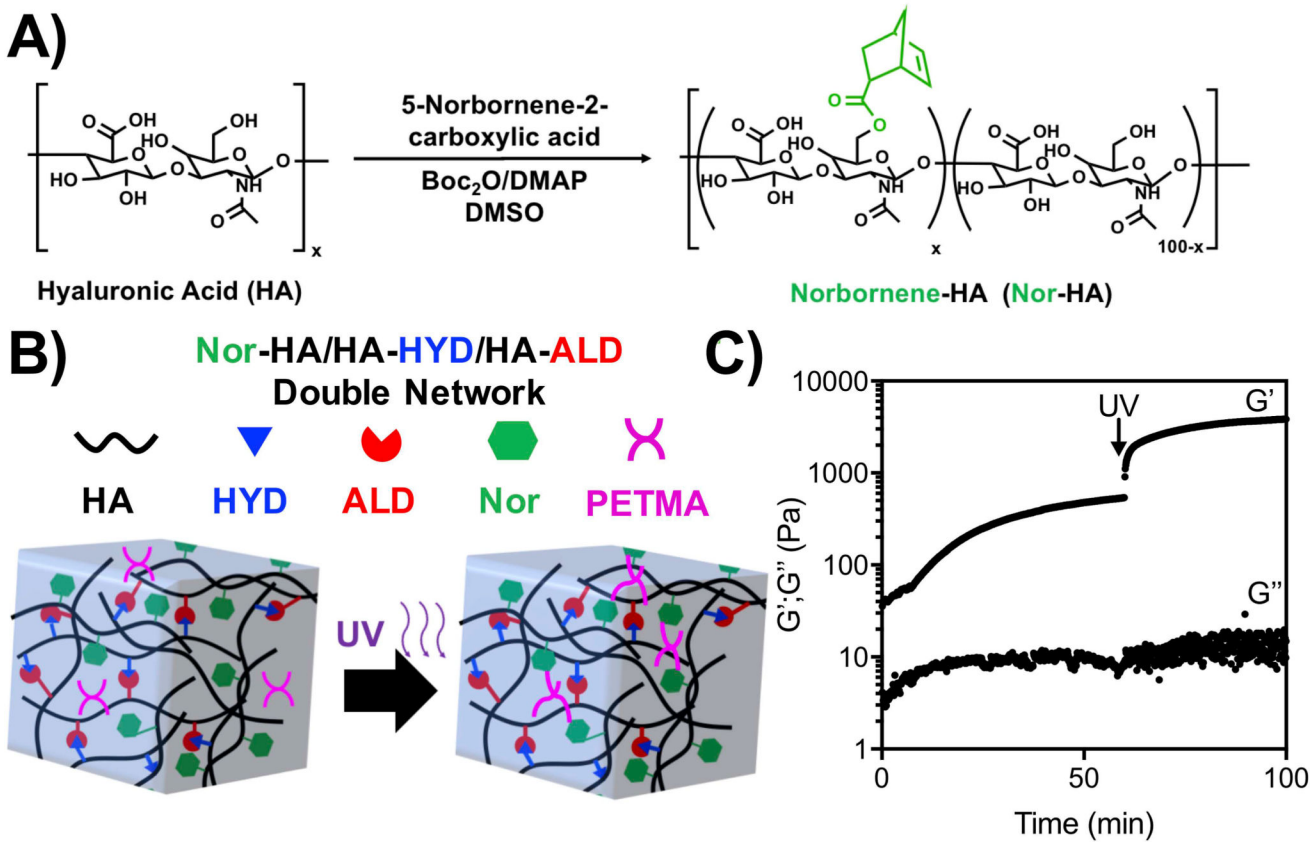

Figure 6. Double-network hydrogels

A) Synthesis schematic of Nor-HA, where norbornenes are introduced through an esterification reaction between 5-norbornene-2-carboxylic acid and the primary alcohol of HA with di-tert-butyl dicarbonate (Boc_2O). B) Schematic of double-networks where Nor-HA is introduced into HYD/ALD hydrogels with a hydrolytically degradable, tetrathiol crosslinker and crosslinked via a thiol-ene reaction in response to UV light and I2959 photoinitiator. C) Photostiffening of networks after UV exposure, demonstrating an increase in G' with shear-oscillatory rheometry.

Author Manuscript Author Manuscript Author Manuscript Author Manuscript

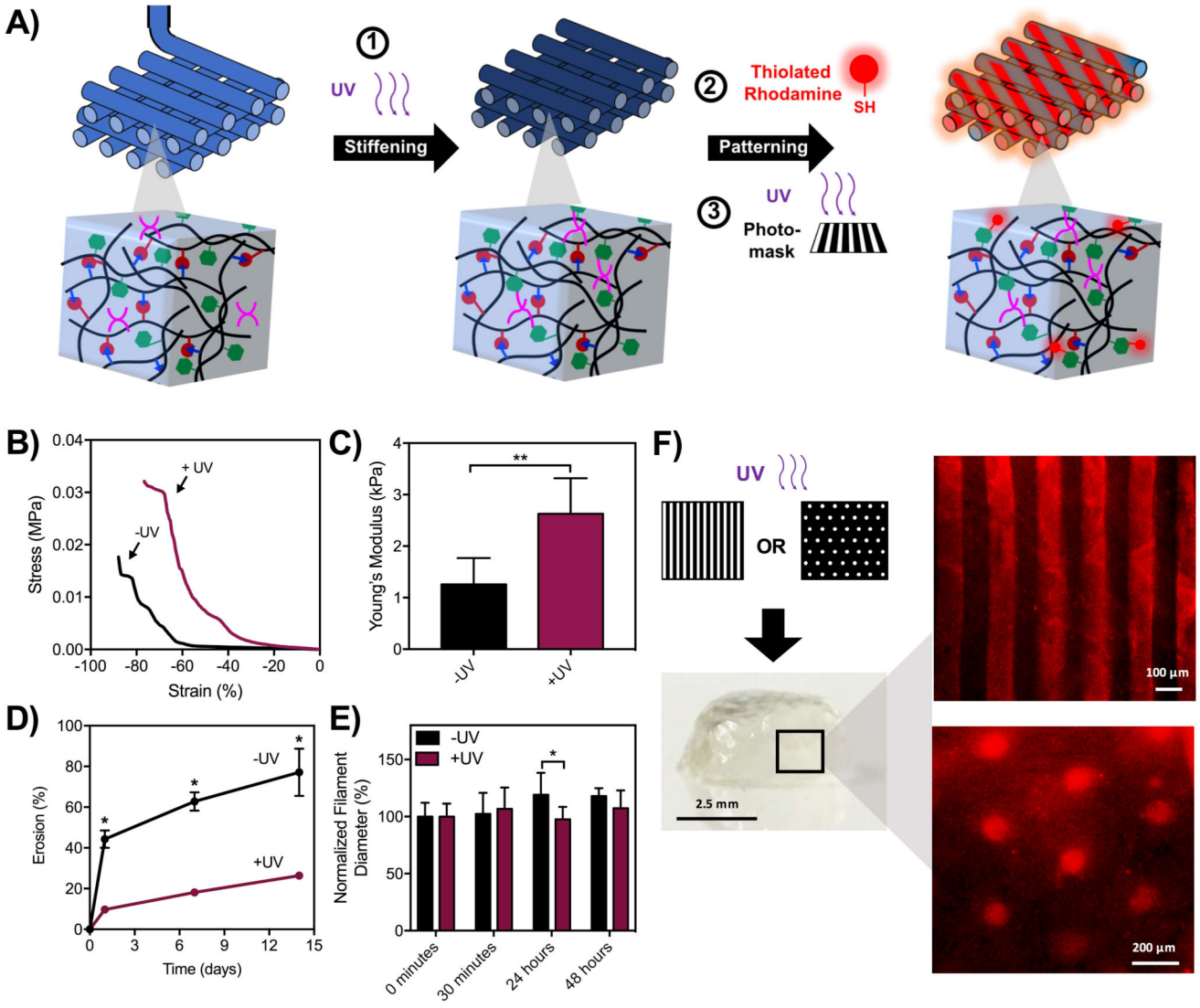

Figure 7. 3D printing of double networks toward orthogonal photostiffening and photopatterning

A) Schematic of sequential photostiffening and photopatterning of double networks. For photostiffening, double network hydrogels were printed with PETMA and I2959 and exposed to UV light (10 mW/cm^2, 2 minutes). For photopatterning, double network hydrogels were incubated with I2959 and thiolated rhodamine and exposed to UV light through a photomask (10 mW/cm^2, 10 minutes). B, C) DMA properties of hydrogel discs before and after photostiffening, $^{**}p<0.01$. D) Erosion of printed double network hydrogel filaments with and without UV irradiation, $^{*}p<0.05$. E) Size of double network filaments (encapsulated with rhodamine-dextran) with and without UV irradiation, $^{*}p<0.05$. F) Hydrogel discs following photopatterning with thiolated rhodamine.